

Subdivision Schemes for the fair Discretization of the Spherical Motion Group

Georg Nawratil and Helmut Pottmann

*Institute of Discrete Mathematics and Geometry, Vienna University of
Technology, Wiedner Hauptstrasse 8-10/104, Vienna, A-1040, Austria*

Abstract

We present two subdivision schemes for the fair discretization of the spherical motion group. The first one is based on the subdivision of the 600-cell according to the tetrahedral/octahedral subdivision scheme of Schaefer, Hakenberg and Warren [Smooth Subdivision of Tetrahedral Meshes. Eurographics Symposium on Geometry Processing (R. Scopigno, D. Zorin, eds.), 151-158, 2004]. The second presented subdivision scheme is based on the spherical kinematic mapping. In the first step we discretize an elliptic linear congruence by the icosahedral discretization of the unit sphere. Then the resulting lines of the elliptic three-space are discretized such that the difference between the maximal and minimal elliptic distance between neighboring grid points becomes minimal.

Key words: spherical motion group, discretization, spherical kinematic mapping, 600-cell, elliptic linear congruence, ...

1 Introduction

Computational mathematics heavily relies on the concept of discretization. It would lead too far to provide a survey of the main application areas of space discretizations. Whereas the discretization of Euclidean spaces is very well understood, the task becomes harder and much less explored if we turn to curved spaces. Recently, a lot of research has been performed on the discretization of two-dimensional surfaces, often in connection with applications in Computer Graphics and Geometric Modeling. However, there appears to be almost no work when we turn to higher dimensional manifolds, especially to the very

Email address: nawratil@geometrie.tuwien.ac.at (Georg Nawratil).

URL: <http://www.geometrie.tuwien.ac.at/nawratil> (Georg Nawratil).

important group SE_3 of Euclidean motions in 3-space. The nasty part here concerns the object orientations, i.e., the discretization of the spherical motion group SO_3 . This is the topic of the present contribution. We are focussing on *fair* discretizations where fairness means regularity. We would like to have a discrete set of positions (elements of SO_3) which are as equally distributed as possible. Thus, we are aiming at a small difference between the largest and the smallest occurring distance of neighboring positions.

We expect that the discretization of the motion group has many applications, e.g. in mechanical simulation tasks or in robotics. Let us sketch here just two application scenarios.

The original motivation for the present paper is the computation of distance fields in the group of rigid body motions with respect to the object-oriented metric introduced by Hofer et al. [5] which takes the mass distribution of the moving body into consideration. Rigid body displacements can be mapped onto points of a 6-dimensional manifold M^6 in the 12-dimensional space of affine mappings. Because the computation of a distance field on M^6 can be decomposed into a translational and a rotational part (see [4]) we are interested in a fair discretization of the spherical motion group. Such distance fields in the group of rigid body motions are of interest for any application, which requires a fast and frequent computation of the distance between a moving object (arbitrary pose) and a given fixed pose. An example for this is the computation of the generalized penetration depth of two overlapping bodies (see [10,15,16]).

Another important application is the fair discretization of a n-dof parallel robots workspace ($n > 2$) with 3 rotational degrees of freedom. A description of the workspace of such a parallel robot can be based on the resulting graph. Nodes are deleted if they do not correspond to reachable configurations. Moreover one has to check if the configurations corresponding to points on the line segments connecting neighboring nodes are singularity-free and self-collision free. If this is not the case then the connection is deleted. Based on the resulting graph a classical motion planner can be used for path planning. According to Merlet [7] the major difficulty is that this description may be quite large, thus the calculation of a trajectory is a time consuming task. Therefore it is important to have an efficient data structure for improving the computation time. Such a data structure for the translational part is trivially obtained by a cubic grid. We will present a fair discretization of SO_3 with nice geometric properties providing such an efficient data structure for the rotational part too. Moreover this scheme can easily be implemented e.g. in Matlab.

Previous work and outline of the present paper

To the best of our knowledge there is no prior work on subdivision schemes for the fair discretization of the spherical motion group. Some related works

are cited and reviewed throughout the paper, which is organized as follows: In Section 2 we repeat fundamentals like unit quaternions and the spherical kinematic mapping. In Section 3 we present a fair discretization of SO_3 based on the subdivision of the 600-cell according to the tetrahedral/octahedral subdivision scheme of Schaefer et al. [13]. At the beginning of section 4 we repeat Clifford parallelity and the concept of the left and right image point of an oriented line. Then we outline a subdivision scheme to generate a fair discretization of an elliptic linear congruence in elliptic three-space E^3 based on the icosahedral discretization of the right unit sphere S^2_- according to Baumgardner and Frederickson [1]¹. In the next step we discretize the lines of this elliptic linear congruence such that we get a fair discretization of E^3 and therefore of SO_3 . We close the paper by comparing and illustrating the presented subdivision schemes in Section 5.

2 Fundamentals

A rotation about the origin (rigid body transformation) in \mathbb{R}^3 is represented with help of an orthogonal matrix \mathbf{R} as $\mathbf{x}' = \mathbf{R}\cdot\mathbf{x}$. The orthogonality condition $\mathbf{R}\cdot\mathbf{R}^T = \mathbf{I}_3$ is a nonlinear constraint on \mathbf{R} , which is not suitable for our task. Therefore we use quaternions to describe the spherical motion group, which leads to a parametrization of the set of orthogonal matrices.

A quaternion $\mathbf{A} = a_0 + a_1i + a_2j + a_3k = (a_0, \mathbf{a})$ with $\mathbf{a} = (a_1, a_2, a_3)$ and $a_0, \dots, a_3 \in \mathbb{R}$ can be considered as the extension of a complex number to four parameters. The imaginary units i, j, k fulfill the following multiplication rules

$$\begin{aligned} i^2 = j^2 = k^2 &= -1 \\ ij = -ji = k, \quad jk &= -kj = i, \quad ki = -ik = j \end{aligned} \quad (1)$$

The set $\mathbb{H} = \mathbb{R}^4$ of all quaternions with addition (componentwise) and multiplication

$$\mathbf{A} \circ \mathbf{B} = (a_0b_0 - \mathbf{a}\cdot\mathbf{b}, a_0\mathbf{b} + b_0\mathbf{a} + \mathbf{a}\times\mathbf{b}) \quad (2)$$

according to the multiplication rules (1) form a skew field. If $\overline{\mathbf{A}} = (a_0, -\mathbf{a})$ denotes the conjugate quaternion to $\mathbf{A} = (a_0, \mathbf{a})$, the Norm $N(\mathbf{A})$ of \mathbf{A} and the multiplicative inverse \mathbf{A}^{-1} is given by:

$$N(\mathbf{A}) = \sqrt{a_0^2 + a_1^2 + a_2^2 + a_3^2} = \sqrt{\mathbf{A} \circ \overline{\mathbf{A}}} \quad \text{and} \quad \mathbf{A}^{-1} := N(\mathbf{A})^{-1}\overline{\mathbf{A}}. \quad (3)$$

A quaternion \mathbf{E} with a norm of one, i.e. $N(\mathbf{E}) = 1$, is called unit quaternion which can be written as $\mathbf{E} = (\cos(\varphi), \sin(\varphi)\mathbf{d})$, where \mathbf{d} is a unit vector. It is

¹ It should be noted that this discretization of the sphere was firstly presented by the architect Buckminster Fuller [2] for the construction of geodesic domes.

well known (see e.g. [8,11,12]), that the mapping $\sigma_{\mathbf{E}} : \mathbf{x} \mapsto \mathbf{x}' = \overline{\mathbf{E}} \circ \mathbf{x} \circ \mathbf{E}$ with the unit quaternion $\mathbf{E} = (\cos(\varphi), \sin(\varphi) \cdot \mathbf{d})$ and $\mathbf{x} \in \mathbb{R}^3$ ($\mathbf{x} = x_1i + x_2j + x_3k$) is a rotation about \mathbf{d} with the angle 2φ . The corresponding rotation matrix \mathbf{R} of $\mathbf{x}' = \mathbf{R}\mathbf{x}$ equals

$$\mathbf{R} = \begin{pmatrix} e_0^2 + e_1^2 - e_2^2 - e_3^2 & 2(e_1e_2 + e_0e_3) & 2(e_1e_3 - e_0e_2) \\ 2(e_1e_2 - e_0e_3) & e_0^2 - e_1^2 + e_2^2 - e_3^2 & 2(e_2e_3 + e_0e_1) \\ 2(e_1e_3 + e_0e_2) & 2(e_2e_3 - e_0e_1) & e_0^2 - e_1^2 - e_2^2 + e_3^2 \end{pmatrix}. \quad (4)$$

The correspondence between unit quaternions and spherical motions is two-to-one and onto, because the two unit quaternions \mathbf{E} and $-\mathbf{E}$ correspond to the same spherical motion $\sigma_{\mathbf{E}}$. The components of one of the two unit quaternions $\pm\mathbf{E}$ are called Euler parameters.

A spherical motion $\sigma_{\mathbf{E}}$ has a well-defined axis and an angle between 0 and π . This angle can also be interpreted as the distance of a given spherical motion to the identity transformation. The angle $\sphericalangle(\sigma_{\mathbf{E}}, \sigma_{\mathbf{F}})$ enclosed by two spherical motions $\sigma_{\mathbf{E}}$ and $\sigma_{\mathbf{F}}$ is defined as the angle of the rotation $\sigma_{\mathbf{C}}$ given by:

$$\frac{\sphericalangle(\sigma_{\mathbf{E}}, \sigma_{\mathbf{F}})}{2} = \arccos\left(\frac{\mathbf{C} + \overline{\mathbf{C}}}{2}\right) \quad \text{with} \quad \mathbf{C} = \overline{\mathbf{E}} \circ \mathbf{F} \quad (5)$$

due to $\overline{\mathbf{C}} \circ [\overline{\mathbf{E}} \circ \mathbf{x} \circ \mathbf{E}] \circ \mathbf{C} = \overline{\mathbf{F}} \circ \mathbf{x} \circ \mathbf{F}$.

The main contribution of this paper is based on the spherical kinematic mapping, which is defined as follows:

Definition 1 $\mathbf{E}\mathbb{R}$ are the homogeneous coordinates of points in P^3 , where \mathbf{E} is a unit quaternion. The mapping $\mathbf{E}\mathbb{R} \mapsto \sigma_{\mathbf{E}}$ of P^3 into the spherical motion group SO_3 is called the spherical kinematic mapping.

The correspondence between $\mathbf{E}\mathbb{R}$ and spherical motions $\sigma_{\mathbf{E}}$ is one-to-one and onto (see [9] and [14]). The distance of points $\mathbf{E}\mathbb{R}$ and $\mathbf{F}\mathbb{R}$ of P^3 is defined as the angle of the corresponding one-dimensional subspaces, i.e.

$$d(\mathbf{E}\mathbb{R}, \mathbf{F}\mathbb{R}) = \sphericalangle(\mathbf{E}\mathbb{R}, \mathbf{F}\mathbb{R}) \in \left[0, \frac{\pi}{2}\right] \quad \text{with} \quad (6)$$

$$\cos \sphericalangle(\mathbf{E}\mathbb{R}, \mathbf{F}\mathbb{R}) = \mathbf{E}^T \mathbf{F} = e_0f_0 + e_1f_1 + e_2f_2 + e_3f_3 = \frac{\overline{\mathbf{E}} \circ \mathbf{F} + \overline{\mathbf{F}} \circ \mathbf{E}}{2}. \quad (7)$$

P^3 endowed with this elliptic metric is an elliptic three-space E^3 . Points $\mathbf{E}\mathbb{R}$ and $\mathbf{F}\mathbb{R}$ of E^3 are called orthogonal (resp. orthogonal quaternions) if $d(\mathbf{E}\mathbb{R}, \mathbf{F}\mathbb{R}) = \frac{\pi}{2}$ holds. Due to (5) the angle $\sphericalangle(\sigma_{\mathbf{E}}, \sigma_{\mathbf{F}})$ is twice the elliptic distance of the points $\mathbf{E}\mathbb{R}$ and $\mathbf{F}\mathbb{R}$ of elliptic three-space E^3 .

3 Discretization of SO_3 based on the subdivision of the 600-Cell

Our first approach for the discretization of SO_3 is based on the fact, that any unit quaternion can be seen as a point on S^3 in \mathbb{R}^4 . Therefore a fair subdivision scheme for discretizing SO_3 can be based on those for S^3 . First of all we review the well-known lowerdimensional case, namely the icosahedral discretization of $S^2 \in \mathbb{R}^3$ (see [1] and [2]).

Icosahedral discretization of S^2

We start with an icosahedron and refine the triangulation by projecting the midpoints of the three edges onto S^2 . Then we connect the resulting points by line segments which yields four smaller triangles (see *Fig. 1*). This procedure can be repeated to generate a mesh of any desired resolution with almost uniformly distributed vertices.

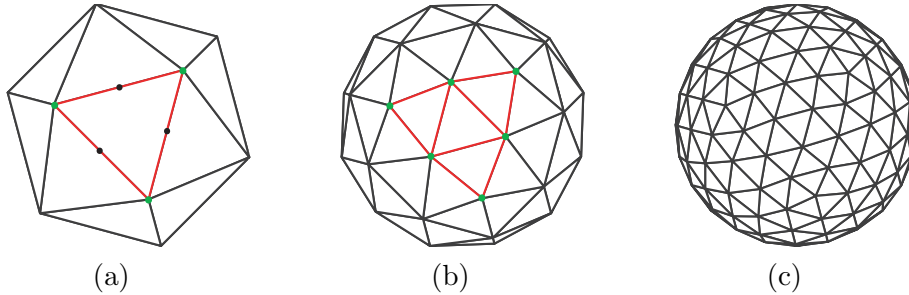


Fig. 1. Icosahedral discretization of S^2 . (a) Icosahedron (b) 1st subdivision step (c) 2nd subdivision step

The number of vertices and the minimal spherical distance $s_i^-(\mathbf{x}, \mathbf{y})$ as well as the maximal spherical distance $s_i^+(\mathbf{x}, \mathbf{y})$ between neighboring vertices \mathbf{x} and \mathbf{y} of the i^{th} subdivision step are given in table 1.

Table 1	# vertices	$s_i^-(\mathbf{x}, \mathbf{y})$	$s_i^+(\mathbf{x}, \mathbf{y})$	$s_i^+ - s_i^-$
i=1	42	31.7175°	36°	4.2825°
i=2	162	15.8587°	18.6994°	2.8407°
i=3	642	7.9294°	9.4443°	1.5149°
i=4	2.562	3.9647°	4.7342°	0.7695°
i=5	10.242	1.9823°	2.3686°	0.3863°
i=6	40.962	0.9912°	1.1845°	0.1933°

The 600-cell

The 4-dimensional analogon of the icosahedron is the 600-cell. The boundary of this Platonic solid is composed of 600 regular tetrahedral cells with 20 meeting at each vertex. Together they form 1200 triangular faces, 720 edges, and 120 vertices. The 600-cell centered at the origin of the unit 4-space has

edges of length φ^{-1} , where $\varphi := \frac{1+\sqrt{5}}{2}$ is the golden ratio. The coordinates of the 120 vertices can be given as follows: The coordinates of 16 vertices are of the form $(\pm\frac{1}{2}, \pm\frac{1}{2}, \pm\frac{1}{2}, \pm\frac{1}{2})$ and the coordinates of 8 vertices correspond to the vertices of the 16-cell, which are obtained from $(\pm 1, 0, 0, 0)$ by permutation. The remaining 96 vertices are obtained by taking even permutations of $\frac{1}{2}(\pm 1, \pm\varphi, \pm\varphi^{-1}, 0)$ (see [3]).

Subdivision scheme for tetrahedra

Because the 600-cell consists of tetrahedral cells we need a subdivision scheme for tetrahedra. The following scheme was suggested by Schaefer et al. [13]: For each tetrahedron we insert new vertices at the midpoints of each edge and connect the vertices together to form four new tetrahedra at the corners of the original one. If we chop these four tetrahedra we get an octahedron (see *Fig. 2 (a)*).

In the next subdivision step we are faced with two kinds of geometric objects, namely tetrahedra and octahedra. Therefore Schaefer et al. defined the following refinement rule for octahedra: We insert vertices at the midpoints of each edge and at the centroid of the octahedron (see *Fig. 2 (b)*). Then we connect the vertices together to form six new octahedra and eight new tetrahedra. The so called tetrahedral/octahedral subdivision scheme is illustrated in *Fig. 2*.

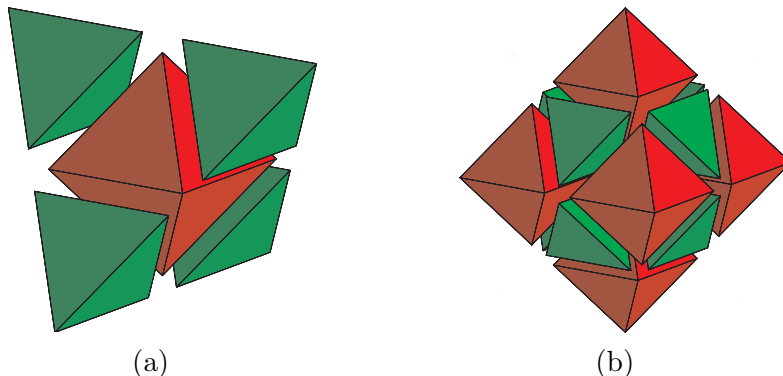


Fig. 2. The tetrahedral/octahedral subdivision scheme: (a) A tetrahedron is split into 4 tetrahedra and one octahedron. (b) An octahedron is split into 6 octahedra and 8 tetrahedra.

3.1 Algorithm for the 600-cell based discretization of S^3

Now we can discretize S^3 by applying the tetrahedral/octahedral subdivision scheme to the tetrahedra of the 600-cell. This can be done as follows:

Our starting configuration is the 600-cell. In each subdivision step we project the midpoint of each edge as well as the centroid of each octahedron onto S^3 . Then we connect the resulting points by line segments as outlined in the tetrahedral/octahedral subdivision scheme. This procedure can again be

repeated to generate a mesh of any desired resolution.

Theorem 1 *The number of tetrahedra ($= T_i$), octahedra ($= O_i$), edges ($= E_i$) and vertices ($= V_i$) of the i^{th} subdivision step of the 600-cell based discretization of S^3 can be computed according to the following recursive formulae:*

$$V_i = V_{i-1} + E_{i-1} + O_{i-1} \quad V_0 = 120 \quad (8)$$

$$E_i = 2 \cdot E_{i-1} + 6 \cdot T_{i-1} + 24 \cdot O_{i-1} \quad E_0 = 720 \quad (9)$$

$$T_i = 4 \cdot T_{i-1} + 8 \cdot O_{i-1} \quad T_0 = 600 \quad (10)$$

$$O_i = T_{i-1} + 6 \cdot O_{i-1} \quad O_0 = 0 \quad (11)$$

Proof: The validity of (8), (10) and (11) follows trivially from the tetrahedral/octahedral subdivision scheme. Equation (9) holds for the following reason: Due to the insertion of vertices at the midpoints of each edge of the $(i-1)^{\text{th}}$ step we get the summand $2 \cdot E_{i-1}$. If we subdivide a tetrahedron we insert at each of its faces 3 new edges. Under the consideration that the resulting 12 edges must be covered twice we get the summand $6 \cdot T_{i-1}$. If we subdivide an octahedron we get 12 new edges through the newly inserted centroid. Moreover, we insert 3 edges in each of its 8 faces which overall results in $(12 + \frac{3 \cdot 8}{2}) \cdot O_{i-1} = 24 \cdot O_{i-1}$. \square

Table 2	T_i	O_i	E_i	V_i
i=1	2.400	600	5.040	840
i=2	14.400	6.000	38.880	6.480
i=3	105.600	50.400	308.160	51.360
i=4	825.600	408.000	2.459.520	409.920
i=5	6.566.400	3.273.600	19.664.640	3.277.440
i=6	52.454.400	26.208.000	157.294.080	26.215.680

Theorem 2 *Each vertex \mathbf{V} ($N(\mathbf{V}) = 1$) of the 600-cell based discretization of S^3 has 12 neighbors, where the neighborhood of a vertex \mathbf{V} is given by the set of all vertices which share a common edge with \mathbf{V} . This holds for each step of the presented subdivision scheme which results in the formula*

$$E_i = 6 \cdot V_i \quad \text{for } i \in \mathbb{N}_0^+. \quad (12)$$

Proof: This statement is valid for the 120 vertices of the 600-cell. Moreover, the number of edges through a vertex \mathbf{V} trivially remains unchanged under the subdivision scheme. Therefore we only have to prove, that each newly inserted point has 12 neighbors. If the newly inserted point is the centroid of an octahedron, then this follows immediately from the considerations given in

the proof of Theorem 1. If the newly inserted point is not a centroid, then it can only be the midpoint of an edge. To complete our proof we have to show that any edge is shared either by (i) 5 tetrahedra or (ii) 2 tetrahedra and 2 octahedra.

ad (i) Assume the line segment connecting the vertex \mathbf{U} and \mathbf{W} is the common edge of t tetrahedra and o octahedra of the i^{th} subdivision step. If we project the midpoint of the common edge of \mathbf{U} and \mathbf{W} up to S^3 we get the point \mathbf{V} . Then the line segment connecting \mathbf{V} and \mathbf{U} resp. \mathbf{V} and \mathbf{W} is still the common edge of t tetrahedra and o octahedra of the $(i+1)^{th}$ subdivision step, due to the proposed subdivision scheme (see *Fig. 2*). This is the reason for the existence of case (i), because our subdivision scheme is based on the 600-cell.

ad (ii) In the last step we consider the newly inserted edges in the faces of the tetrahedra resp. octahedra. Such a face can only be shared by 2 octahedra, 2 tetrahedra or 1 octahedron and 1 tetrahedron, respectively. In each of these three cases the newly inserted edges in the faces share 2 tetrahedra and 2 octahedra according to *Fig. 2*. \square

We implemented the outlined subdivision scheme for the discretization of the spherical motion group in Matlab. The maximal elliptic distance $d_i^+(\mathbf{X}\mathbb{R}, \mathbf{Y}\mathbb{R})$ as well as the minimal elliptic distance $d_i^-(\mathbf{X}\mathbb{R}, \mathbf{Y}\mathbb{R})$ of neighboring point pairs \mathbf{X} and \mathbf{Y} of the i^{th} subdivision step are given in table 3 for $i = 1, \dots, 6$.

Table 3	d_i^-	d_i^+	$d_i^+ - d_i^-$		d_i^-	d_i^+	$d_i^+ - d_i^-$
i=1	18°	18.6994°	0.6994°	i=4	2.25°	2.3773°	0.1273°
i=2	9°	9.4767°	0.4767°	i=5	1.125°	1.1888°	0.0638°
i=3	4.5°	4.7505°	0.2505°	i=6	0.5625°	0.5949°	0.0324°

4 Elliptic linear congruence based discretization of SO_3

Beside the fairness of the discretization of SO_3 , the implementation of such subdivision schemes as well as the data processing of the resulting grid points are further important aspects for application. In practice one deals with a large amount of data, e.g. fair discretization of a n -dof workspace (see Section 1), and therefore an efficient data structure providing fast access is of interest. This can be achieved by the following subdivision scheme for discretizing SO_3 . First of all we outline a subdivision scheme to generate a fair discretization of an elliptic linear congruence in E^3 based on the icosahedral discretization of S^2 . In the next step we discretize the lines of this elliptic linear congruence such that we get a fair discretization of E^3 and therefore of SO_3 .

4.1 Left and Right Image Point of an Oriented Line and Clifford Parallelity

If an oriented line $\vec{\mathbf{L}} \in E^3$ is spanned by orthogonal points $\mathbf{E}\mathbb{R}$ and $\mathbf{F}\mathbb{R}$ with $N(\mathbf{E}) = N(\mathbf{F}) = 1$, then the Plücker coordinates $(\mathbf{l}, \hat{\mathbf{l}})$ of $\vec{\mathbf{L}}$ with $l_{jk} = e_j f_k - e_k f_j$ are normalized, i.e. $\mathbf{l}^2 + \hat{\mathbf{l}}^2 = 1$. With the help of the orthogonal unit quaternions \mathbf{E} and \mathbf{F} the oriented line $\vec{\mathbf{L}}$ can be parametrized as $\mathbf{L}(\varphi)\mathbb{R}$, where the unit quaternion $\mathbf{L}(\varphi)$ is given by:

$$\mathbf{L}(\varphi) = \cos(\varphi)\mathbf{E} - \sin(\varphi)\mathbf{F} \quad \text{with } \varphi \in [0, \pi]. \quad (13)$$

Assume a point $\mathbf{X}\mathbb{R} \notin \vec{\mathbf{L}}$ with $N(\mathbf{X}) = 1$ is given and $\vec{\mathbf{L}}$ is parametrized as in (13). Then the closest point $\mathbf{C}\mathbb{R}$ to $\mathbf{X}\mathbb{R}$ on $\vec{\mathbf{L}}$ with respect to the elliptic metric (6) is uniquely determined by

$$\varphi_{\mathbf{C}} := -\arctan\left(\frac{\mathbf{X}^T \mathbf{F}}{\mathbf{X}^T \mathbf{E}}\right). \quad (14)$$

Definition 2 If $\vec{\mathbf{L}} \in P^3$ is an oriented line with normalized Plücker coordinates $(\mathbf{l}, \hat{\mathbf{l}})$, e.i. $\mathbf{l}^2 + \hat{\mathbf{l}}^2 = 1$, then the left and right image points of $\vec{\mathbf{L}}$ are defined as:

$$\begin{aligned} \mu^+ : (\mathbf{l}, \hat{\mathbf{l}}) &\mapsto \mathbf{l}^+ := \mathbf{l} + \hat{\mathbf{l}} \dots \dots \text{left image point of } \vec{\mathbf{L}} \\ \mu^- : (\mathbf{l}, \hat{\mathbf{l}}) &\mapsto \mathbf{l}^- := \mathbf{l} - \hat{\mathbf{l}} \dots \dots \text{right image point of } \vec{\mathbf{L}} \end{aligned} \quad (15)$$

\mathbf{l}^+ and \mathbf{l}^- are unit vectors because $(\mathbf{l}, \hat{\mathbf{l}})$ is normalized. Therefore μ^+ resp. μ^- maps the space of oriented lines onto the so called left resp. right unit sphere, which is denoted by S_+^2 resp. S_-^2 .

Remark: It can be shown that if $\vec{\mathbf{L}} \in P^3$ is incident with a point $\mathbf{E}\mathbb{R}$, then the spherical motion $\sigma_{\mathbf{E}}$ takes $\vec{\mathbf{L}}$'s left image point to its right image point: $\sigma_{\mathbf{E}}(\mathbf{l}^+) = \mathbf{l}^-$. Conversely, the points of P^3 which correspond to the spherical motions transforming $\mathbf{x} \in S^2$ to $\mathbf{y} \in S^2$, comprise a line $\vec{\mathbf{L}} := (\mathbf{x} + \mathbf{y}, \mathbf{x} - \mathbf{y})$. For details see [11].

Definition 3 Two oriented lines $\vec{\mathbf{G}}$ and $\vec{\mathbf{L}}$ of P^3 are called left resp. right Clifford parallel if $\mathbf{g}^+ \times \mathbf{l}^+ = \mathbf{o}$ resp. $\mathbf{g}^- \times \mathbf{l}^- = \mathbf{o}$ holds.

It follows immediately from the intersection condition of Sommerville ($\mathbf{g} \cdot \hat{\mathbf{l}} + \hat{\mathbf{g}} \cdot \mathbf{l} = 0$) which can be written as $\mathbf{g}^+ \cdot \mathbf{l}^+ - \mathbf{g}^- \cdot \mathbf{l}^- = 0$ that Clifford parallel lines have never a common point. Moreover, it can be shown (e.g. see [11]) that the minimum distance of any point on $\vec{\mathbf{L}}$ to its (left or right) Clifford parallel $\vec{\mathbf{G}}$ is the same for all points. Therefore Clifford parallels are equidistant. This result leads to the following definition:

Definition 4 The distance $d(\vec{\mathbb{L}}, \vec{\mathbb{G}})$ between the Clifford parallel lines $\vec{\mathbb{L}}$ and $\vec{\mathbb{G}}$ is defined as the minimum elliptic distance of any point on $\vec{\mathbb{L}}$ to $\vec{\mathbb{G}}$.

4.2 Fair Discretization of the elliptic linear congruence

Without loss of generality, we assume $\mathbf{I}^+ = (0, 0, 1)$ and $\mathbf{I}^- = (a, b, c)$ with $\|\mathbf{I}^-\| = 1$. The lines $\vec{\mathbb{L}}$ with Plücker coordinates $\mathbf{l} = (a, b, 1 + c)$ and $\hat{\mathbf{l}} = (-a, -b, 1 - c)$ are contained in two linear line complexes given by

$$l_{01} + l_{23} = 0 \quad \text{and} \quad l_{02} + l_{31} = 0.$$

The pencil of linear line complexes spanned by $(\mathbf{c}_1, \hat{\mathbf{c}}_1) = (1, 0, 0, 1, 0, 0)\mathbb{R}$ and $(\mathbf{c}_2, \hat{\mathbf{c}}_2) = (0, 1, 0, 0, 1, 0)\mathbb{R}$ intersect the Plücker quadric, which is given by $l_{01}l_{23} + l_{02}l_{31} + l_{03}l_{12} = 0$, in two complex conjugate points $(1, i, 0, 1, i, 0)\mathbb{C}$ and $(1, -i, 0, 1, -i, 0)\mathbb{C}$. These points correspond to the skew pair of complex conjugate focal lines of the elliptic linear congruence. Therefore the fibers of μ^+ (Def. 2) are an elliptic linear congruence. Moreover for $\mathbf{I}^+ = (0, 0, 1)$ the fibers of μ^+ are also the fibers of the Hopf mapping (see [6] and [11]).

As a consequence the discretization of the elliptic linear congruence can be done by discretizing the right unit sphere S^2_- . Therefore the set of lines $\vec{\mathbb{L}}_j := (\mathbf{I}_j^+, \mathbf{I}_j^-)$ of the i^{th} subdivision step of the elliptic linear congruence discretization can be given as follows:

Without loss of generality we set $\mathbf{I}_j^+ := (0, 0, 1)$ for all j . The unit vector \mathbf{I}_j^- are the position vectors of the vertices of the i^{th} subdivision step of the S^2_- discretization according to Baumgardner and Frederickson [1]. Therefore the number of lines j of the i^{th} step of the elliptic linear congruence discretization equals the number of vertices of the i^{th} step of the icosahedral discretization of S^2 , which is given in table 1 for $i = 1, \dots, 6$. The neighborhood of a line $\vec{\mathbb{L}}$ of the elliptic linear congruence discretization is induced by the icosahedral discretization of S^2_- as follows:

Definition 5 The line $\vec{\mathbb{L}}$ corresponds to a vertex \mathbf{l} of the discretization of the right unit sphere S^2_- . Each line which corresponds to a vertex of the icosahedral discretization of S^2_- sharing a common edge with \mathbf{l} is a neighboring line of $\vec{\mathbb{L}}$.

Remark: The distance $d(\vec{\mathbb{L}}, \vec{\mathbb{G}})$ between two lines $\vec{\mathbb{L}}$ and $\vec{\mathbb{G}}$ of the elliptic linear congruence discretization is half the spherical distance $s(\mathbf{l}, \mathbf{g})$ of the corresponding vertices \mathbf{l} and \mathbf{g} of $\vec{\mathbb{L}}$ and $\vec{\mathbb{G}}$ of the discretized right unit sphere S^2_- . Moreover it should be noted that only the lines which correspond to the 12 vertices of the icosahedron have 5 neighboring lines. All other lines of the discretized elliptic linear congruence have six neighboring lines.

4.3 Starting configuration and line discretization

In the starting configuration of our algorithm the right unit sphere S^2_- is discretized by the icosahedron. Therefore the 0^{th} step of the discretized elliptic linear congruence consists of 12 lines $\vec{\mathcal{L}}_i$ ($i = 1, \dots, 12$). It is possible to discretize each line $\vec{\mathcal{L}}_i$ by 5 Points $\mathbf{P}_i^1\mathbb{R}, \dots, \mathbf{P}_i^5\mathbb{R}$ such that the resulting configuration (60 Points $\mathbf{P}_1^1\mathbb{R}, \dots, \mathbf{P}_{12}^5\mathbb{R}$) corresponds to the 120 vertices of the 600-cell. This can easily be done as follows:

We discretize the line $\vec{\mathcal{L}}_1$ by 5 points $\mathbf{P}_1^1\mathbb{R}, \dots, \mathbf{P}_1^5\mathbb{R}$ with $d(\mathbf{P}_1^j\mathbb{R}, \mathbf{P}_1^{j+1}\mathbb{R}) = d(\mathbf{P}_1^1\mathbb{R}, \mathbf{P}_1^5\mathbb{R}) = \frac{\pi}{5}$ for $j = 1, \dots, 4$. Then we compute for each neighboring line $\vec{\mathcal{L}}_n$ of $\vec{\mathcal{L}}_1$ the two points $\mathbf{P}_n^1\mathbb{R}$ and $\mathbf{P}_n^2\mathbb{R}$ with $d(\mathbf{P}_1^1\mathbb{R}, \mathbf{P}_n^1\mathbb{R}) = d(\mathbf{P}_1^5\mathbb{R}, \mathbf{P}_n^2\mathbb{R}) = \frac{\pi}{5}$. Moreover the elliptic distance between $\mathbf{P}_n^1\mathbb{R}$ and $\mathbf{P}_n^2\mathbb{R}$ is also $\frac{\pi}{5}$. Then we discretize the lines $\vec{\mathcal{L}}_n$ analogously to the line $\vec{\mathcal{L}}_1$ and iterate this procedure until all 12 lines are discretized. Therefore each point of the resulting configuration has 12 neighbors (closest points) at the elliptic distance of $\frac{\pi}{5}$. Trivially the 120 points $\pm\mathbf{P}_1^1, \dots, \pm\mathbf{P}_{12}^5$ with $N(\pm\mathbf{P}_1^1) = \dots = N(\pm\mathbf{P}_{12}^5) = 1$ correspond to the 120 vertices of the 600-cell.

Based on this starting configuration we give a subdivision scheme for generating a fair discretization of E^3 . Due to the outlined discretization of the elliptic linear congruence it is clear how to insert new lines in each subdivision step. But how should these lines be discretized? In order to come up with an answer we have to make the following considerations.

Definition 6 *The discretized version $\mathcal{L} := \{\mathbf{P}^1, \dots, \mathbf{P}^k\}$ of the line $\vec{\mathcal{L}} \in E^3$ is called regular if*

$$d(\mathbf{P}^u, \mathbf{P}^{u+1}) = d(\mathbf{P}^k, \mathbf{P}^1) = \frac{\pi}{k} \quad \text{with } u = 1, \dots, k-1 \quad \text{and } k \geq 2 \quad \text{holds.}$$

It should be noted that the 12 lines of our starting configuration are regular discretized lines. In the next step we define the distance between two regular discretized Clifford parallel lines analogously to the smooth case (see Def. 4).

Definition 7 *The distance $d(\mathcal{L}_i, \mathcal{L}_j)$ of regular discretized Clifford parallel lines $\mathcal{L}_i := \{\mathbf{P}_i^1, \dots, \mathbf{P}_i^m\}$ and $\mathcal{L}_j := \{\mathbf{P}_j^1, \dots, \mathbf{P}_j^n\}$ is defined as*

$$d(\mathcal{L}_i, \mathcal{L}_j) := \min_{l \in \{1, \dots, n\}} \left(d(\mathbf{P}_i^a\mathbb{R}, \mathbf{P}_j^l\mathbb{R}) \right) \quad \text{with } a \in \{1, \dots, m\}. \quad (16)$$

Lemma 1 *The distance of Def. 7 is symmetric (e.i. $d(\mathcal{L}_i, \mathcal{L}_j) = d(\mathcal{L}_j, \mathcal{L}_i)$) and independent of the selected point $\mathbf{P}_i^a \in \mathcal{L}_i$ if and only if:*

General case: $m = n$

Special case A: $2m = n \wedge d(\mathcal{L}_i, \mathcal{L}_j) = \arccos \left(\cos \left(d(\vec{\Gamma}_i, \vec{\Gamma}_j) \right) \cos \left(\frac{\pi}{2n} \right) \right)$

Special case B: $m = 2n \wedge d(\mathcal{L}_i, \mathcal{L}_j) = \arccos \left(\cos \left(d(\vec{\Gamma}_i, \vec{\Gamma}_j) \right) \cos \left(\frac{\pi}{2m} \right) \right)$

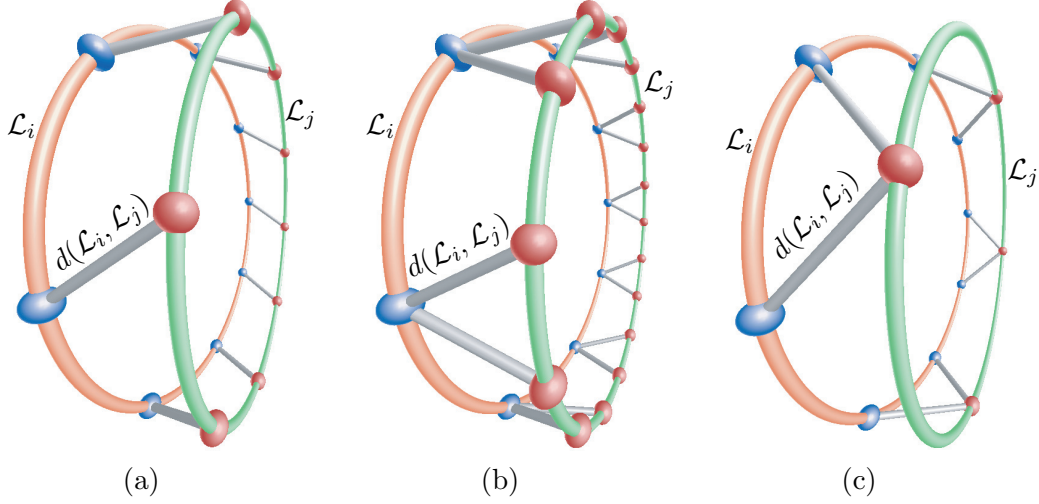


Fig. 3. (a) General case (b) Special case A (c) Special case B

Proof: The validity of this Lemma is trivial and it can immediately be seen from Fig. 3, where the general case and the special cases are illustrated. \square

Moreover it should be noted that the distance between two regular discretized Clifford parallel lines \mathcal{L}_i and \mathcal{L}_j of the general case is bounded by:

$$d(\mathcal{L}_i, \mathcal{L}_j) \in \left[d(\vec{\Gamma}_i, \vec{\Gamma}_j), \arccos \left(\cos \left(d(\vec{\Gamma}_i, \vec{\Gamma}_j) \right) \cos \left(\frac{\pi}{2n} \right) \right) \right] \quad (17)$$

The natural claim

Assume the regular discretized lines \mathcal{L}_i and \mathcal{L}_j with $n := \# \mathcal{L}_i = \# \mathcal{L}_j$ which correspond to neighboring vertices l_i and l_j of the icosahedron are given. If we project the midpoint of l_i and l_j onto S^2_- we get the point $l_{i,j}$, which corresponds to the line $\vec{\Gamma}_{i,j}$ of E^3 . Due to $d(\vec{\Gamma}_i, \vec{\Gamma}_{i,j}) = d(\vec{\Gamma}_j, \vec{\Gamma}_{i,j})$ we claim that $d(\mathcal{L}_i, \mathcal{L}_{i,j})$ equals $d(\mathcal{L}_j, \mathcal{L}_{i,j})$.

Now the question arises if there exists always a regular discretization of $\vec{\Gamma}_{i,j}$ such that the above condition is fulfilled and if yes, would it be unique. As a consequence of the special cases in Lemma 1 we have to distinguish between the following three cases:

Case A: $d(\mathcal{L}_i, \mathcal{L}_j) \neq d(\vec{\mathcal{L}}_i, \vec{\mathcal{L}}_j)$, $d(\mathcal{L}_i, \mathcal{L}_j) \neq \arccos\left(\cos\left(d(\vec{\mathcal{L}}_i, \vec{\mathcal{L}}_j)\right)\cos\left(\frac{\pi}{2n}\right)\right)$

In this case there always exist two schemes for the regular discretization of $\vec{\mathcal{L}}_{i,j}$, which are called minimal distance line discretization and maximal distance line discretization (see *Fig. 4*). The discretization can be done as follows: Take any point $\mathbf{P}_i\mathbb{R} \in \mathcal{L}_i$ and its uniquely determined closest point $\mathbf{P}_j\mathbb{R} \in \mathcal{L}_j$. For both point $\mathbf{P}_i\mathbb{R}, \mathbf{P}_j\mathbb{R}$ compute the closest point $\mathbf{C}_i\mathbb{R}$ and $\mathbf{C}_j\mathbb{R}$ on $\vec{\mathcal{L}}_{i,j}$ according to (14). Then there exist two orthogonal points $\mathbf{M}_1\mathbb{R}$ and $\mathbf{M}_2\mathbb{R}$ on $\vec{\mathcal{L}}_{i,j}$ with $d(\mathbf{M}_u\mathbb{R}, \mathbf{C}_i\mathbb{R}) = d(\mathbf{M}_u\mathbb{R}, \mathbf{C}_j\mathbb{R})$ ($u = 1, 2$). Without loss of generality we assume $d(\mathbf{M}_1\mathbb{R}, \mathbf{C}_i\mathbb{R}) < d(\mathbf{M}_2\mathbb{R}, \mathbf{C}_i\mathbb{R})$ and $N(\mathbf{M}_1) = N(\mathbf{M}_2) = 1$. Due to the assumptions of case A the case $d(\mathbf{M}_1\mathbb{R}, \mathbf{C}_i\mathbb{R}) = d(\mathbf{M}_2\mathbb{R}, \mathbf{C}_j\mathbb{R})$ does not exist. According to (13) the line $\vec{\mathcal{L}}_{i,j}$ can be regularly discretized as follows:

- Minimal distance line discretization:

$$\mathcal{L}_{i,j}^- := \left\{ \cos\left(\frac{i\pi}{n}\right)\mathbf{M}_1 - \sin\left(\frac{i\pi}{n}\right)\mathbf{M}_2 \mid i = 0, \dots, n-1 \right\} \quad (18)$$

- Maximal distance line discretization:

$$\mathcal{L}_{i,j}^+ := \left\{ \cos\left(\frac{(2i+1)\pi}{2n}\right)\mathbf{M}_1 - \sin\left(\frac{(2i+1)\pi}{2n}\right)\mathbf{M}_2 \mid i = 0, \dots, n-1 \right\} \quad (19)$$

Moreover it should be noted that both schemes are independent of the choice of the point $\mathbf{P}_i\mathbb{R} \in \mathcal{L}_i$. Trivially the following relation holds:

$$d(\mathcal{L}_i, \mathcal{L}_{i,j}^-) = d(\mathcal{L}_j, \mathcal{L}_{i,j}^-) < d(\mathcal{L}_i, \mathcal{L}_{i,j}^+) = d(\mathcal{L}_j, \mathcal{L}_{i,j}^+).$$

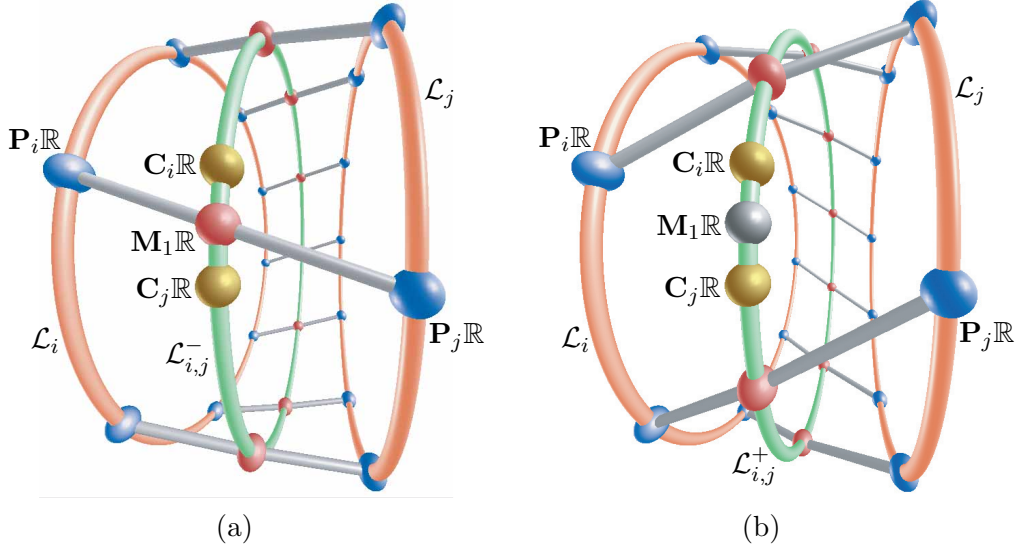


Fig. 4. Line discretization schemes of case A: (a) Minimal distance line discretization $\mathcal{L}_{i,j}^-$ (b) Maximal distance line discretization $\mathcal{L}_{i,j}^+$

Case B: $d(\mathcal{L}_i, \mathcal{L}_j) = d(\vec{\mathcal{L}}_i, \vec{\mathcal{L}}_j)$

The same considerations as in case A lead to $\mathbf{C}_i\mathbb{R} = \mathbf{C}_j\mathbb{R} = \mathbf{M}_1\mathbb{R}$ and we can apply the minimal line discretization scheme $\mathcal{L}_{i,j}^-$ of (18) (see Fig. 5 (a)) and the maximal line discretization scheme $\mathcal{L}_{i,j}^+$ of (19) (see Fig. 5 (b)), respectively. But now we get two more fair discretizations of $\vec{\mathcal{L}}_{i,j}$ if n is even and $n \geq 4$ (see Fig. 6):

- Special case 1:

$$\mathcal{L}_{i,j}^{S_1} := \left\{ \cos\left(\frac{(2i+1)\pi}{n}\right) \mathbf{M}_1 - \sin\left(\frac{(2i+1)\pi}{n}\right) \mathbf{M}_2 \mid i = 0, \dots, \frac{n}{2} - 1 \right\} \quad (20)$$

- Special case 2:

$$\mathcal{L}_{i,j}^{S_2} := \left\{ \cos\left(\frac{(2i-1)\pi}{n}\right) \mathbf{M}_1 - \sin\left(\frac{(2i-1)\pi}{n}\right) \mathbf{M}_2 \mid i = 0, \dots, \frac{n}{2} - 1 \right\} \quad (21)$$

These two definitions depend on the choice of the point $\mathbf{P}_i\mathbb{R} \in \mathcal{L}_i$ which is clear from $\mathcal{L}_{i,j}^{S_1} \cup \mathcal{L}_{i,j}^{S_2} = \mathcal{L}_{i,j}^+$. Moreover we get

$$d(\mathcal{L}_i, \mathcal{L}_{i,j}^-) < d(\mathcal{L}_i, \mathcal{L}_{i,j}^+) = d(\mathcal{L}_i, \mathcal{L}_{i,j}^{S_1}) = d(\mathcal{L}_i, \mathcal{L}_{i,j}^{S_2}).$$

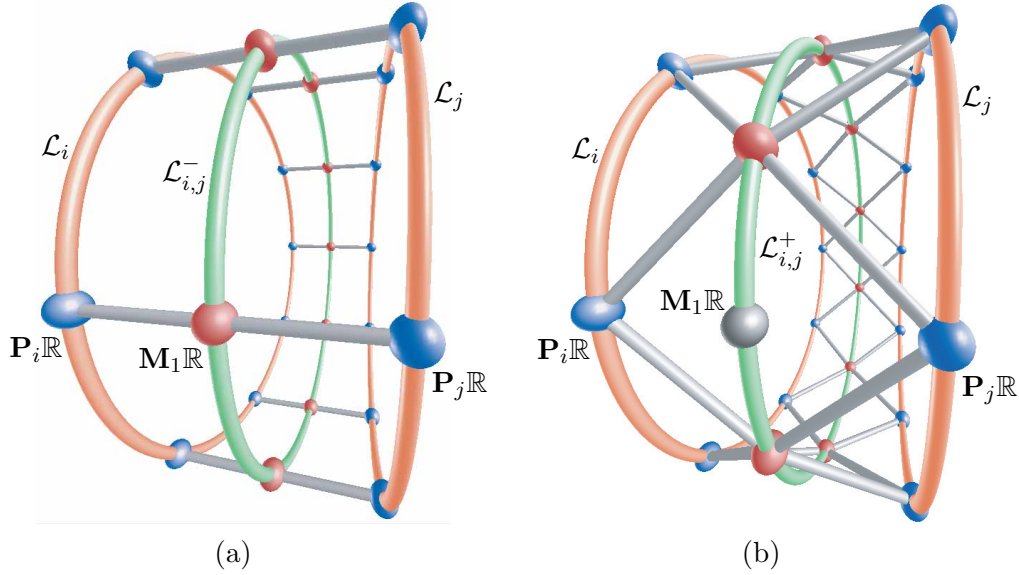


Fig. 5. Line discretization schemes of case B: (a) Minimal distance line discretization $\mathcal{L}_{i,j}^-$ (b) Maximal distance line discretization $\mathcal{L}_{i,j}^+$

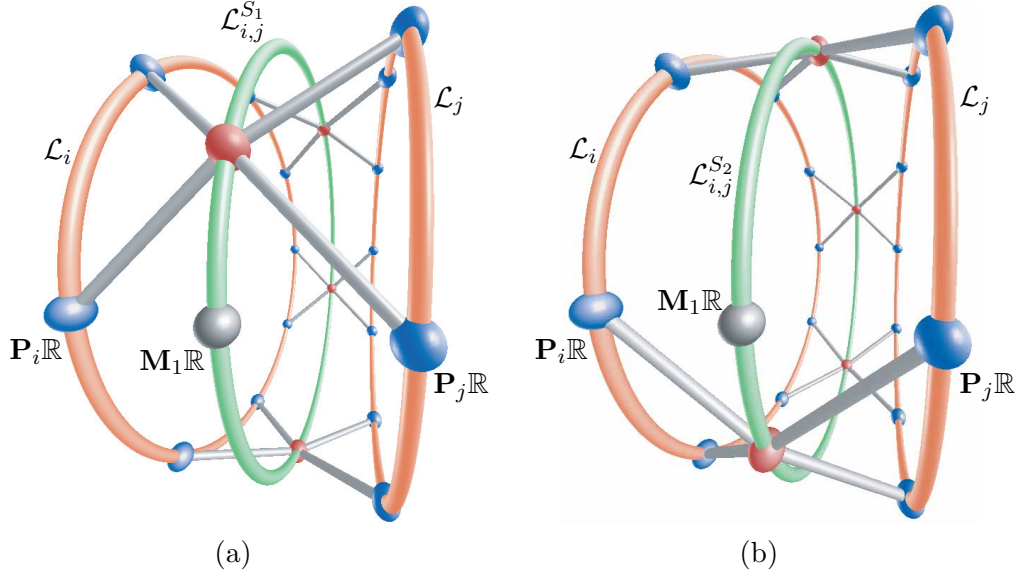


Fig. 6. Line discretization schemes of case B: (a) Special case 1 (b) Special case 2

Case C: $d(\mathcal{L}_i, \mathcal{L}_j) = \arccos \left(\cos \left(d(\vec{\mathcal{L}}_i, \vec{\mathcal{L}}_j) \right) \cos \left(\frac{\pi}{2n} \right) \right)$

In this case any point $\mathbf{P}_i^R \in \mathcal{L}_i$ has two closest points $\mathbf{P}_j^a \in \mathcal{L}_j$ and $\mathbf{P}_j^b \in \mathcal{L}_j$. In dependency of \mathbf{P}_j^a and \mathbf{P}_j^b we get the orthogonal point pairs $\mathbf{M}_1^a, \mathbf{M}_2^a$ and $\mathbf{M}_1^b, \mathbf{M}_2^b$ on $\vec{\mathcal{L}}_{i,j}$. Only if $n = 2$ the point \mathbf{M}_1^x is not determined uniquely due to $d(\mathbf{M}_1^x, \mathbf{C}_i) = d(\mathbf{M}_2^x, \mathbf{C}_i)$ with $x \in \{a, b\}$. Then there are the following three possibilities for the discretization of $\vec{\mathcal{L}}_{i,j}$:

$$\mathcal{L}_{i,j}^a := \{\mathbf{M}_1^a, \mathbf{M}_2^a\}, \quad \mathcal{L}_{i,j}^b := \{\mathbf{M}_1^b, \mathbf{M}_2^b\}, \quad \mathcal{L}_{i,j}^S := \mathcal{L}_{i,j}^a \cup \mathcal{L}_{i,j}^b.$$

For $n > 2$ we can apply to both pairs the minimal and maximal line discretization scheme of (18) and (19), which leads to $\mathcal{L}_{i,j}^{-a}, \mathcal{L}_{i,j}^{+a}$ and $\mathcal{L}_{i,j}^{-b}, \mathcal{L}_{i,j}^{+b}$ (see Fig. 7). Due to $d(\mathbf{M}_1^a, \mathbf{M}_1^b) = \frac{\pi}{2n}$ we get $\mathcal{L}_{i,j}^{\pm} := \mathcal{L}_{i,j}^{+a} = \mathcal{L}_{i,j}^{-b}$ and $\mathcal{L}_{i,j}^{\mp} := \mathcal{L}_{i,j}^{-a} = \mathcal{L}_{i,j}^{+b}$. Therefore we cannot distinguish between these two line discretization schemes in this case. Moreover there is a third possibility for a regular discretization of $\vec{\mathcal{L}}_{i,j}$ namely $\mathcal{L}_{i,j}^S := \mathcal{L}_{i,j}^{\pm} \cup \mathcal{L}_{i,j}^{\mp}$ (see Fig. 7). However the following relation holds

$$d(\mathcal{L}_i, \mathcal{L}_{i,j}^{\pm}) = d(\mathcal{L}_i, \mathcal{L}_{i,j}^{\mp}) = d(\mathcal{L}_i, \mathcal{L}_{i,j}^S).$$

The last preparatory work which must be done is the definition of the neighborhood of a grid point. Such a definition should be based on the definition of neighboring lines (see Def. 5) and it should induce the same neighborhood for a grid point of the starting configuration as it is done by the edges of the 600-cell. If we take this into consideration we end up with the following definition:

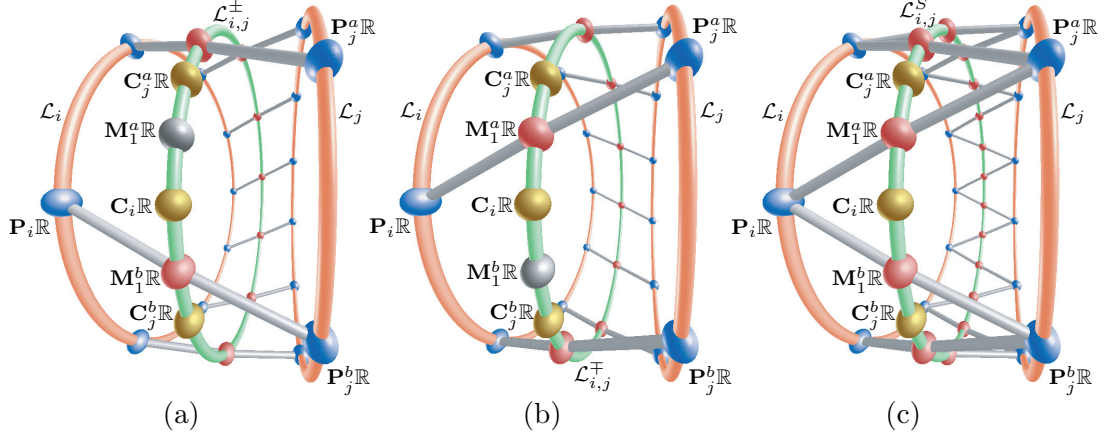


Fig. 7. Line discretization schemes of case C: (a) $\mathcal{L}_{i,j}^{\pm} := \mathcal{L}_{i,j}^{+a} = \mathcal{L}_{i,j}^{-b}$ (b) $\mathcal{L}_{i,j}^{\mp} := \mathcal{L}_{i,j}^{-a} = \mathcal{L}_{i,j}^{+b}$ (c) $\mathcal{L}_{i,j}^S := \mathcal{L}_{i,j}^{\pm} \cup \mathcal{L}_{i,j}^{\mp}$

Definition 8 $\mathcal{L}_j := \{\mathbf{P}_i^1\mathbb{R}, \dots, \mathbf{P}_i^{k_i}\mathbb{R}\}$ for $i = 1, \dots, n$ are the regular discretized neighboring lines of the regular discretized line $\mathcal{L}_0 := \{\mathbf{P}_0^1\mathbb{R}, \dots, \mathbf{P}_0^{k_0}\mathbb{R}\}$ according to Def. 5. Then the set \mathcal{N}_j of neighboring points on \mathcal{L}_j with respect to \mathbf{P}_0^i is defined as

$$\mathcal{N}_j := \left\{ \mathbf{P}_j^k\mathbb{R} \mid d(\mathbf{P}_0^i\mathbb{R}, \mathbf{P}_j^k\mathbb{R}) = \min_{k \in \{1, \dots, k_i\}} (d(\mathbf{P}_0^i\mathbb{R}, \mathbf{P}_j^k\mathbb{R})) \right\}.$$

Then the neighborhood $\mathcal{N}_{\mathbf{P}_0^i}$ of $\mathbf{P}_0^i\mathbb{R}$ is given by $\mathcal{N}_{\mathbf{P}_0^i} := \bigcup_{j=0}^n \mathcal{N}_j$ where

$$\mathcal{N}_0 := \left\{ \mathbf{P}_0^k\mathbb{R} \mid d(\mathbf{P}_0^i\mathbb{R}, \mathbf{P}_0^k\mathbb{R}) = \min_{k \in \{1, \dots, k_0\} \setminus i} (d(\mathbf{P}_0^i\mathbb{R}, \mathbf{P}_0^k\mathbb{R})) \right\}$$

are the neighbors of \mathbf{P}_0^i on its carrier line.

Remark It should be noted that the set \mathcal{N}_0 always consists of two elements if k_0 is greater than 2. The set \mathcal{N}_j for $j = 1, \dots, n$ only consists of 2 elements if $k_0 = k_j$ and $d(\mathcal{L}_0, \mathcal{L}_j) = \arccos\left(\cos\left(d(\vec{\mathcal{L}}_i, \vec{\mathcal{L}}_j)\right) \cos\left(\frac{\pi}{2k_0}\right)\right)$ or if $2k_0 = k_j$ and $d(\mathcal{L}_0, \mathcal{L}_j) = \arccos\left(\cos\left(d(\vec{\mathcal{L}}_i, \vec{\mathcal{L}}_j)\right) \cos\left(\frac{\pi}{2k_j}\right)\right)$.

4.4 Algorithm for the elliptic linear congruence based discretization of SO_3

Now we can give the complete algorithm for the discretization of the spherical motion group based on the discretization of the elliptic linear congruence.

0. Compute the 60 points of the starting configuration.
1. Double the number of points on each regular discretized line \mathcal{L}^i of the i^{th} step such that it is still regular. Moreover the resulting point set \mathcal{L}^{i+1} should contain \mathcal{L}^i .
2. Insert the new lines according to the subdivision scheme for the discretization of the elliptic linear congruence (see section 4.2).
3. Discretize each of the new lines according to one of the possible line discretization schemes of case A, B and C. Then compute the difference between the maximal and minimal distance between neighboring grid points of the $(i + 1)^{\text{th}}$ step of all possible combinatorial cases induced by the different line discretization schemes. The combination which cause the minimal difference is our new starting configuration.

In the next step we show that we can neglect the special cases, which reduces the number of combinatorial cases of step 3. We will show this only up to the 6^{th} subdivision step because the corresponding grid has a resolution of more than 13 millions points, which is more than sufficient for any computation.

Theorem 3 *The combinatorial cases in which the line discretization schemes $\mathcal{L}_{i,j}^{S_1}$, $\mathcal{L}_{i,j}^{S_2}$ or $\mathcal{L}_{i,j}^S$ are applied to the newly inserted lines of the i^{th} subdivision step, cannot minimize the difference between the maximal and minimal distance between neighboring grid points of the resulting grid. ($i = 1, \dots, 6$)*

Proof: If we exclude the line discretization schemes $\mathcal{L}_{i,j}^{S_1}$, $\mathcal{L}_{i,j}^{S_2}$ and $\mathcal{L}_{i,j}^S$ each regular discretized line \mathcal{L}_i of the i^{th} subdivision step carries the same number of grid points, namely $5 \cdot 2^i$. Due to (17) we can give easily the upper bound b_i^+ and the lower bound b_i^- of the distance between neighboring grid points of the i^{th} subdivision step as follows:

$$b_i^- := \min\left(\frac{s_i^-}{2}, \frac{\pi}{5 \cdot 2^i}\right), \quad b_i^+ := \max\left(\arccos\left(\cos\left(\frac{s_i^+}{2}\right) \cos\left(\frac{\pi}{5 \cdot 2^{i+1}}\right)\right), \frac{\pi}{5 \cdot 2^i}\right)$$

with s_i^+ and s_i^- according to table 1 for $i = 1, \dots, 6$. If we would apply the line discretization scheme $\mathcal{L}_{i,j}^{S_1}$ or $\mathcal{L}_{i,j}^{S_2}$ to one of the newly inserted lines $\vec{\Gamma}_{i,j}$ of the i^{th} subdivision step the set of all distances between two neighboring grid points contains the value $\frac{\pi}{5 \cdot 2^{i-1}}$, which is the distance between two neighboring points on $\mathcal{L}_{i,j}$. For the line discretization scheme $\mathcal{L}_{i,j}^S$ this set contains the value $\frac{\pi}{5 \cdot 2^{i+1}}$. Moreover this set contains the value $\frac{\pi}{5 \cdot 2^i}$, which corresponds to the distance between neighboring points on the lines of the starting configuration. As outlined in table 4 the inequalities $\frac{\pi}{5 \cdot 2^{i-1}} - \frac{\pi}{5 \cdot 2^i} = \frac{\pi}{5 \cdot 2^i} > b_i^+ - b_i^-$ and $\frac{\pi}{5 \cdot 2^i} - \frac{\pi}{5 \cdot 2^{i+1}} = \frac{\pi}{5 \cdot 2^{i+1}} > b_i^+ - b_i^-$ are valid for $i = 1, \dots, 6$ and therefore the theorem is proven. \square

Table 4	b_i^-	b_i^+	$b_i^+ - b_i^-$	$\frac{\pi}{5 \cdot 2^{i+1}}$	$\frac{\pi}{5 \cdot 2^{i-1}}$
i=1	15.8587°	20.0577°	4.1990°	9°	18°
i=2	7.9294°	10.3676°	2.4382°	4.5°	9°
i=3	3.9647°	5.2297°	1.2650°	2.25°	4.5°
i=4	1.9823°	2.6207°	0.6384°	1.125°	2.25°
i=5	0.9912°	1.3111°	0.3199°	0.5625°	1.125°
i=6	0.4956°	0.6556°	0.1600°	0.28125°	0.5625°

Moreover this result guarantees that for two neighboring lines $\mathcal{L}_{i,j}$ and $\mathcal{L}_{i,k}$ the distance $d(\mathcal{L}_{i,j}, \mathcal{L}_{i,k})$ is well defined due to the fact that each line carries the same number of grid points. Therefore we can already compute the number of grid points $D_i \cdot P_i$ of the i^{th} subdivision step, where D_i denotes the number of regular discretized lines and P_i the number of points per line. The corresponding values are given in table 5 for $i = 1, \dots, 6$.

Table 5	D_i	P_i	$D_i \cdot P_i$		D_i	P_i	$D_i \cdot P_i$
i=1	42	10	420	i=4	2562	80	204.960
i=2	162	20	3.240	i=5	10242	160	1.638.720
i=3	642	40	25.680	i=6	40962	320	13.107.840

Remark: It is surprising that the total number $\frac{V_i}{2}$ of spherical motions of the i^{th} discretization step of SO_3 based on the subdivision of the 600-cell (see table 2) equals the number of spherical motions of the i^{th} discretization step of SO_3 based on the elliptic linear congruence (see table 5). As a consequence we can easily compare the two discretization schemes by the difference of the maximal and minimal elliptic distance of neighboring grid points.

Extended natural claim

In order to reduce the number of combinatorial cases we expand the natural claim to the whole discretized elliptic linear congruence. Assume that the neighboring pairs \vec{L}_i, \vec{L}_j and \vec{L}_k, \vec{L}_l with $d(\vec{L}_i, \vec{L}_j) = d(\vec{L}_k, \vec{L}_l)$ are given. Then the discretized lines should fulfill the condition $d(\mathcal{L}_i, \mathcal{L}_j) = d(\mathcal{L}_k, \mathcal{L}_l)$, which is true for the starting configuration.

Then the number of combinatorial cases of the i^{th} subdivision step equals:

$$\text{step 0} \xrightarrow{2^1} \text{step 1} \xrightarrow{2^2} \text{step 2} \xrightarrow{2^5} \text{step 3} \xrightarrow{2^{15}} \text{step 4} \xrightarrow{2^{51}} \text{step 5} \xrightarrow{2^{187}} \text{step 6}$$

Under this reasonable claim we can prove the following theorem. We will do this again up to the 6th subdivision step due to the more than sufficient resolution of the resulting grid.

Theorem 4 *It is possible to apply to each newly inserted line $\vec{\Gamma}_{i,j}$ the maximum distance line discretization scheme $\mathcal{L}_{i,j}^+$. The resulting maximum distance subdivision scheme minimizes the difference between the maximal and minimal distance between the grid points of the i^{th} subdivision step with respect to the extended natural claim. ($i = 1, \dots, 6$)*

Proof: (i) First we have to check if in each iteration step the maximal distance line discretization is possible or if the indistinguishable schemes $\mathcal{L}_{i,j}^+$ and $\mathcal{L}_{i,j}^-$ must be applied. After we doubled the number of points of the discretized lines of the $(i-1)^{\text{th}}$ step we only have to check if case C occurs. Fortunately it turns out by computation that this is not the case up to the 6^{th} step. Thus we can apply the unique determined maximal distance line discretization scheme to each newly inserted line up to the 6^{th} step. Therefore the maximal distance subdivision scheme trivially fulfills our extended natural claim.

(ii) Perhaps the proof of the second part of this theorem can also be done explicitly up to the 3^{rd} or 4^{th} step by computing all possible combinatorial cases and comparing the difference between the maximal and minimal distance between the resulting grid points. But for the 5^{th} and 6^{th} subdivision step these does not make sense due to the enormous number of combinatorial cases. Therefore we will give the following elegant proof:

Proof for $i = 1$: All 30 newly inserted lines can be discretized according to the maximal or minimal distance line discretization scheme. Computation yields that the difference between maximal and minimal distance of neighboring grid points of the maximal distance subdivision scheme is 0.4860° . For the other combinatorial case we get the value 2.6273° . It should be noted that the minimal distance $d_1^- = 18^\circ$ between grid points of the maximal distance subdivision scheme occurs between neighboring points of the same carrier line.

Proof for $i = 2, \dots, 5$: First of all we compute the maximal distance d_i^+ and the minimal distance d_i^- between neighboring grid points of the i^{th} subdivision step of the maximal distance subdivision scheme. Due to the validity of $d_i^- < \frac{\pi}{5 \cdot 2^i} < d_i^+$ (see table 7) the maximal and minimal distance occurs between points of neighboring lines. It turns out that the discretized lines $\mathcal{L}_{i,a}^+, \mathcal{L}_{i,b}^+, \mathcal{L}_{i,c}^+, \mathcal{L}_{i,d}^+$ causing the maximal and minimal distance lie in a similar configuration for $i = 2, \dots, 5$. This configuration is illustrated via the corresponding points on the right unit sphere S_-^2 in Fig. 8 and Fig. 9.

Now we apply to the lines of the configuration all other combinatorial cases induced by the maximal and minimal line discretization scheme. We have to differentiate between the following three cases:

$$(a) \mathcal{L}_{i,a}^-, \mathcal{L}_{i,b}^+, \mathcal{L}_{i,c}^-, \mathcal{L}_{i,d}^+ \quad (b) \mathcal{L}_{i,a}^+, \mathcal{L}_{i,b}^-, \mathcal{L}_{i,c}^+, \mathcal{L}_{i,d}^- \quad (c) \mathcal{L}_{i,a}^-, \mathcal{L}_{i,b}^-, \mathcal{L}_{i,c}^-, \mathcal{L}_{i,d}^- \quad (22)$$

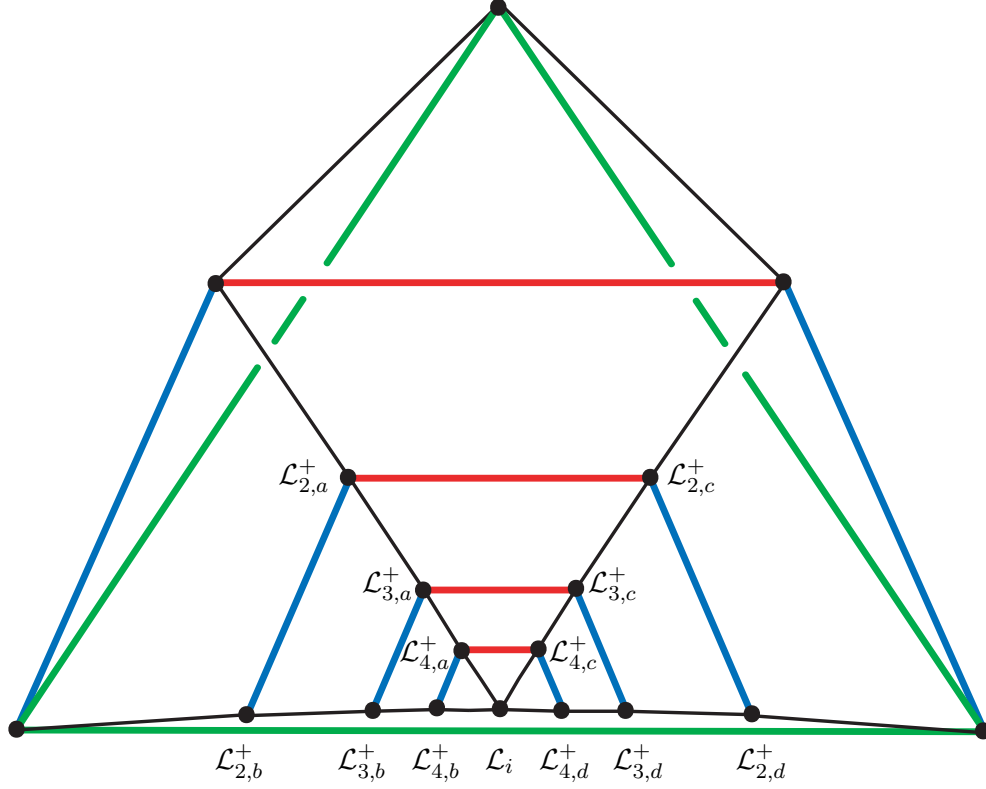


Fig. 8. The corresponding points on S_-^2 of the configuration $\mathcal{L}_{i,a}^+, \mathcal{L}_{i,b}^+, \mathcal{L}_{i,c}^+, \mathcal{L}_{i,d}^+$ for $i = 1, \dots, 4$. Blue edges indicate the minimal distance and red edges the maximal distance. The edges of the initial icosahedral face are colored green.

All other cases can be excluded because the extended natural claim implies that the maximal and minimal line discretization schemes have to operate on the corresponding points of S_-^2 with respect to the extended icosahedral group determined by the icosahedron of step 0. As a consequence we cannot improve the maximal distance $d_i^+ := d(\mathcal{L}_{i,a}^+, \mathcal{L}_{i,c}^+) = d(\mathcal{L}_{i,a}^-, \mathcal{L}_{i,c}^-)$. Therefore the above three cases can only improve the minimal distance $d_i^- := d(\mathcal{L}_{i,a}^+, \mathcal{L}_{i,b}^+) = d(\mathcal{L}_{i,c}^+, \mathcal{L}_{i,d}^+)$. But for the combinatorial case (a) the inequality $d(\mathcal{L}_{i,a}^-, \mathcal{L}_{i,b}^+) < d_i^-$ holds for $i = 2, \dots, 5$ (see table 6). For the combinatorial cases (b) and (c) the inequality $d(\mathcal{L}_{i,b}^-, \mathcal{L}_i) < d_i^-$ holds for $i = 2, \dots, 5$ (see table 6) and therefore this part is proven.

Table 6	d_i^-	$d(\mathcal{L}_{i,a}^-, \mathcal{L}_{i,b}^+)$	$d(\mathcal{L}_{i,b}^-, \mathcal{L}_i)$
i=2	8.8864°	8.2763°	7.9294°
i=3	4.3816°	4.2147°	3.9647°
i=4	2.1741°	2.1252°	1.9823°
i=5	1.0827°	1.0669°	0.9912°
i=6	0.5402°	0.5345°	0.4956°

Proof for $i = 6$:

Similar considerations as in the above case lead us to the configuration $\mathcal{L}_{6,a}^+, \mathcal{L}_{6,b}^+, \mathcal{L}_{6,c}^+, \mathcal{L}_{6,d}^+, \mathcal{L}_{6,e}^+, \mathcal{L}_{6,f}^+$ (Fig. 9) with $d_6^+ := d(\mathcal{L}_{6,e}^+, \mathcal{L}_{6,f}^+)$ and $d_6^- := d(\mathcal{L}_{6,a}^+, \mathcal{L}_{6,b}^+) = d(\mathcal{L}_{6,c}^+, \mathcal{L}_{6,d}^+)$. Due to the extended natural claim we have to check the same three cases as in (22) for $i = 6$. Again we cannot improve d_i^+ . Moreover for the cases (b) and (c) the inequality $d(\mathcal{L}_{6,b}^-, \mathcal{L}_6^-) < d_6^-$ holds. Case (a) also cannot improve d_i^- due to $d(\mathcal{L}_{6,a}^-, \mathcal{L}_{6,b}^-) < d_6^-$ (see table 6). \square

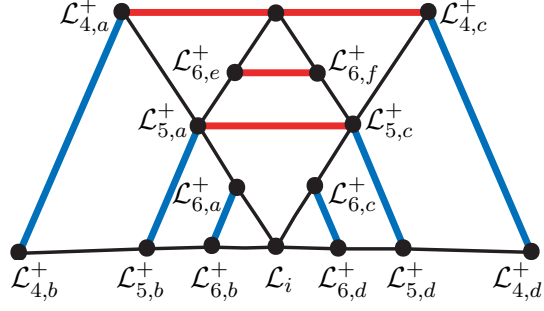


Fig. 9. The corresponding points on S^2 of the configuration $\mathcal{L}_{i,a}^+, \mathcal{L}_{i,b}^+, \mathcal{L}_{i,c}^+, \mathcal{L}_{i,d}^+, \mathcal{L}_{6,e}^+, \mathcal{L}_{6,f}^+$ for $i = 4, \dots, 6$. Blue edges indicate the minimal distance and red edges the maximal distance.

Table 7	d_i^-	d_i^+	$d_i^+ - d_i^-$		d_i^-	d_i^+	$d_i^+ - d_i^-$
i=1	18°	18.4860°	0.4860°	i=4	2.1741°	2.6074°	0.4333°
i=2	8.8864°	9.9594°	1.0730°	i=5	1.0827°	1.3064°	0.2237°
i=3	4.3816°	5.1396°	0.7580°	i=6	0.5402°	0.6544°	0.1142°

The maximal and minimal elliptic distance of neighboring grid points generated by the maximal distance subdivision scheme are outlined in table 7.

5 Comparison of the presented subdivision schemes

The elliptic linear congruence based grid of step 1 is fairer than the one obtained by the subdivision of the 600-cell and the grids of step 2 to 6 are less fair than those based on the subdivision of the 600-cell (compare table 3 and table 7). Recall that fairness is meant in the sense of regularity. A further difference between the grids generated by these two methods is the number of neighboring grid points. Due to Theorem 2 each grid point of the 600-cell based discretization of SO_3 has 12 neighbors. The neighborhood of a grid point of the elliptic linear congruence based discretization of SO_3 depends on the carrier line of this point, because all points of one line have exactly the same neighborhood. Due to the formula given in the remark of section 4.3 the number of neighbors can easily be determined. It turns out by computation that the following holds up to the 6th subdivision step:

- Grid points on the 12 lines of our starting configuration have 12 neighbors. It should be noted that this is true for any step of the maximal distance subdivision scheme and not only up to step 6.
- Grid points on lines which correspond to points on S^2_- placed on geodesics between neighboring vertices of the starting icosahedron have 10 neighbors.
- All other grid points have 8 neighbors.

5.1 Data structure

Clearly, the 600-cell based subdivision scheme implies a hierarchical data structure. Due to this structure the neighboring grid points to an arbitrary given spherical motion \mathbf{X} with $N(\mathbf{X}) = 1$ can easily be determined as follows: First one has to check in which of the 600 cells \mathbf{X} is located. Then one has to test within which geometric object of the next subdivision step \mathbf{X} lies. Depending on the resolution of the grid this procedure must be repeated until one ends up with the information that \mathbf{X} is located in the tetrahedron T or the octahedron O of the i^{th} subdivision step. In the general case the four vertices of T or the six vertices of O are the searched neighboring grid points of \mathbf{X} . It should be noted that this hierarchical data structure can not be implemented so easily (e.g. in Matlab), because an efficient implementation must consider that the spherical motion group is covered twice by the resulting grid.

In the contrary the elliptic linear congruence based discretization of SO_3 implies the following nice matrix data structure: The unit quaternions of the obtained grid points of the i^{th} subdivision step can be stored in a $D_i \times P_i \times 4$ array, where D_i is the number of regular discretized lines and P_i the number of points per line. Beside the information of neighboring lines which can be stored in a 12×5 and a $(D_i - 12) \times 6$ array, one only needs to save the neighbors of one point per line because the neighborhood of all other points of the same line are given by the geometric properties of the grid. This results in a very compact and efficient data structure which is suited for implementation e.g. in Matlab and provides fast access (computation time). Moreover the additional information of the hierarchical data structure of the icosahedral discretization of S^2_- also provides a fast computation of the neighboring grid points to an arbitrary given spherical motion \mathbf{XR} . First one has to compute the uniquely determined line \vec{X} of the elliptic linear congruence through \mathbf{XR} . Then the (in general three) closest regular discretized grid lines to \vec{X} can easily be obtained by \vec{X} 's right image point and the hierarchical data structure of the icosahedral discretization of S^2_- . In the last step one only has to find the closest grid points on these lines to \mathbf{XR} .

Summarizing, we can say that both schemes have their advantages, thus the choice of the right one depends on the respective application.

5.2 Visualization

We apply the spherical motions which correspond to the grid points of the presented subdivision schemes to an oriented line segment tangential to the unit sphere. The chosen projection direction of all the following images equals $\mathbf{1}_j^+ = (0, 0, 1)$. Therefore the rotational symmetry of the elliptic linear congruence based subdivision scheme can be seen immediately.

In *Fig. 10* the 60 poses of the line segment corresponding to the vertices of the 600-cell (=starting configuration) are illustrated.

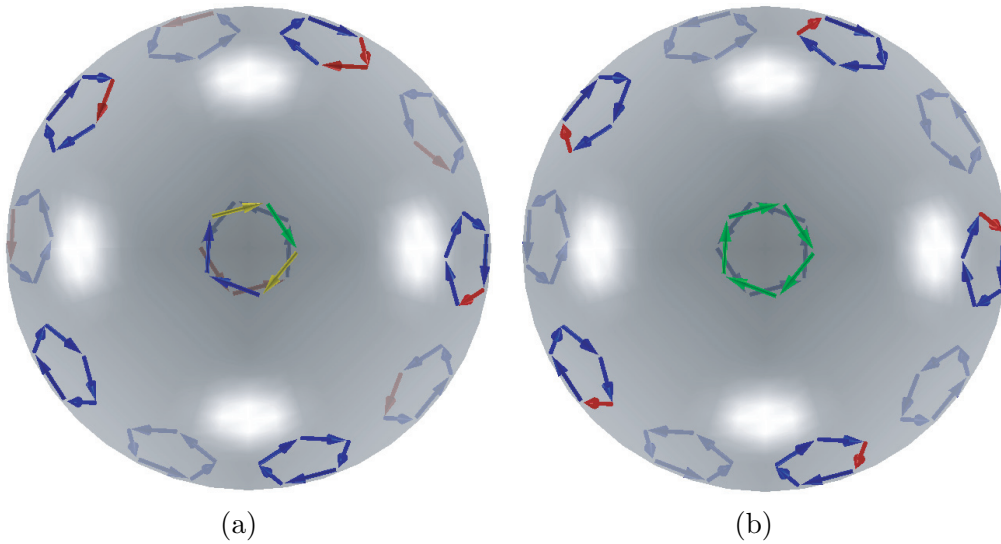


Fig. 10. Starting configuration: (a) Neighborhood of the green line segment: The yellow ones correspond to the grid points of \mathcal{N}_0 (see Def. 8). All other neighbors are colored red. (b) The grid points which correspond to the green (red) line segments belong to a regular discretized line of the starting configuration.

In *Fig. 11* the poses of the oriented line segment which correspond to the grid points of the 1st step of the presented schemes are illustrated. The red ones (with green arrowheads) correspond to the newly inserted grid points and the blue ones (with yellow arrowheads) to the points of the starting configuration.

The grid points of the 2nd step of the presented schemes are illustrated via the corresponding poses of the oriented line segment in *Fig. 12*. Blue ones belong to the starting configuration, green ones to the newly inserted grid points of the 1st step and yellow ones (with red arrowheads) to the newly inserted grid points of the 2nd step.

It should be noted that illustrating higher steps of the subdivision schemes does not make sense from the graphical point of view. Even in *Fig. 12* it is difficult to differentiate visually between the displayed line segments.

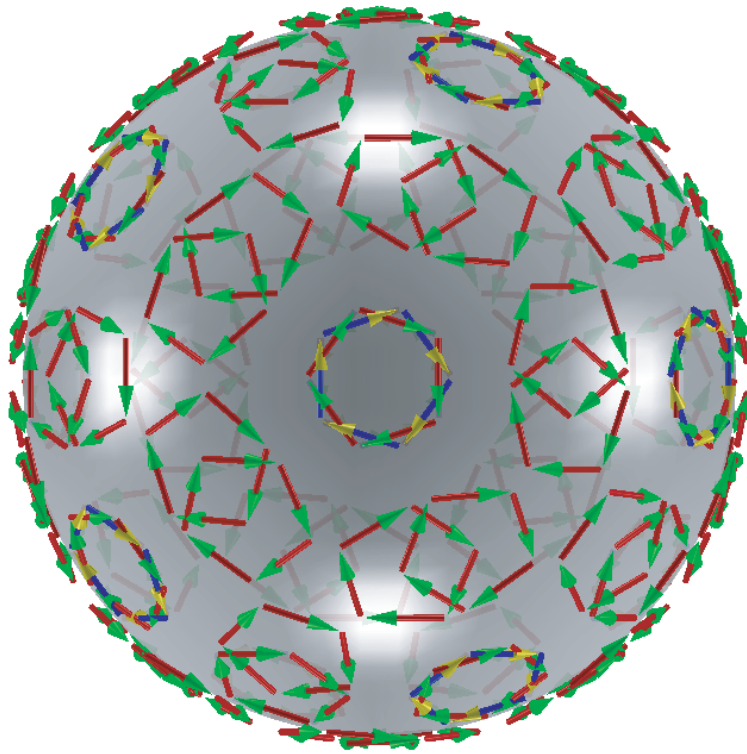
6 Conclusion

We presented a fair discretization of SO_3 based on the subdivision of the 600-cell according to the tetrahedral/octahedral subdivision scheme of Schaefer et al. [13]. We proved that each grid point has 12 neighbors in any subdivision step and computed the difference between the maximal and minimal elliptic distance of neighboring grid points.

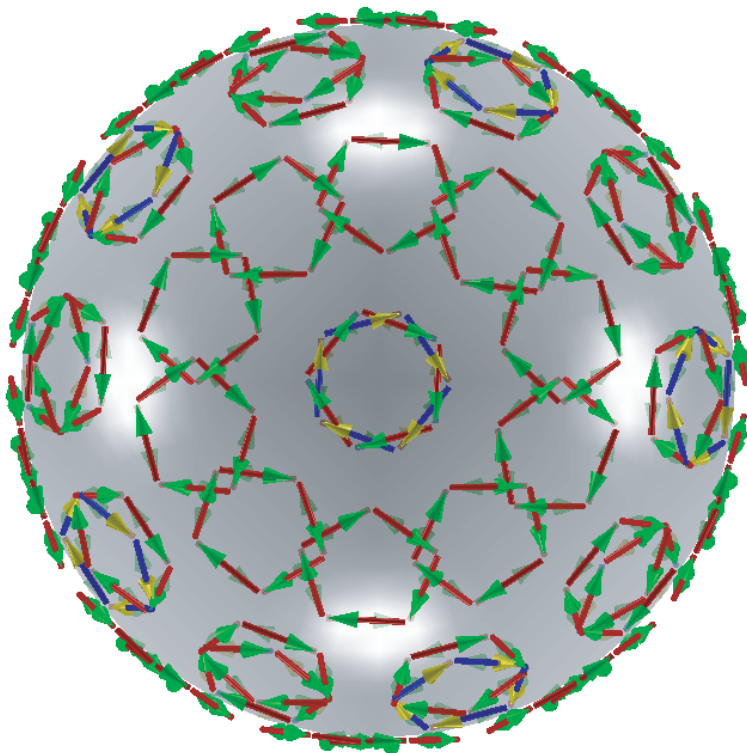
The main contribution of this paper is based on the spherical kinematic mapping. We presented a subdivision scheme to generate a fair discretization of an elliptic linear congruence in the elliptic three-space. This discretization is done by the icosahedral discretization of the right unit sphere. Under consideration of the extended natural claim postulated in section 4.4, we discretized the lines of the discretized elliptic linear congruence such that the difference between the maximal and minimal elliptic distance of neighboring grid points becomes minimal. Moreover we proved that the maximal distance subdivision scheme is the fairest one up to the 6th subdivision step fulfilling this claim.

Although these two presented discretizations are totally different they result in the same number of spherical motions in each subdivision step. Therefore we can compare the two schemes by the difference of the maximal and minimal elliptic distance of neighboring grid points. It turns out that the elliptic linear congruence based grid of step 1 is fairer than the one obtained by the subdivision of the 600-cell. The grids of step 2 to 6 are less fair than those based on the subdivision of the 600-cell. A further difference between the grids obtained by these two methods is the number of neighboring grid points, because a point of the elliptic linear congruence based grid can have 12, 10 or 8 neighbors.

Beside the fairness of the discretization of SO_3 , the implementation of such subdivision schemes as well as the data processing of the resulting grid points are further important aspects for application. Contrary to the 600-cell based subdivision scheme implying a hierarchical data structure the elliptic linear congruence based grid provides a compact and efficient matrix data structure. Both structures have their advantages, thus the choice of the right subdivision scheme depends on the respective application.

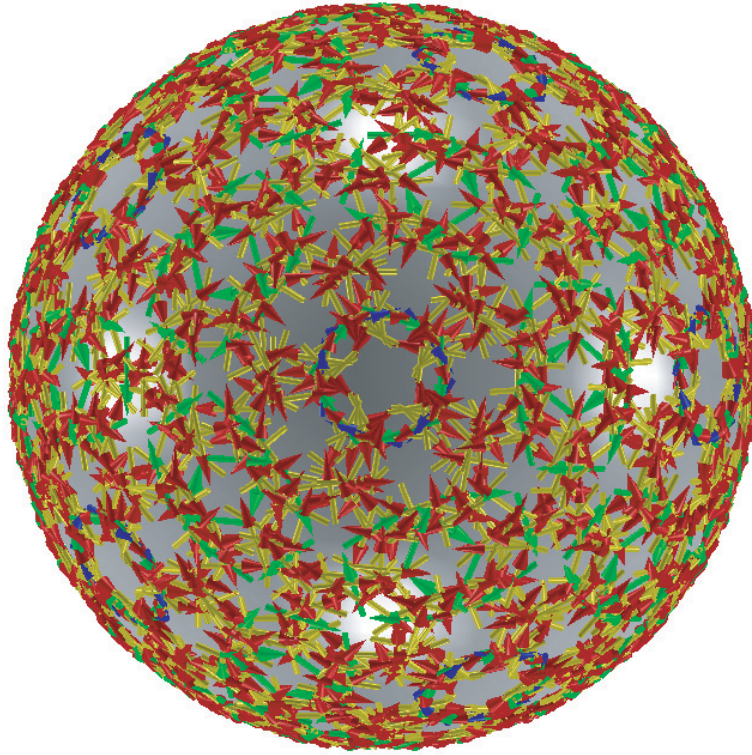


(a) 600-cell based subdivision scheme.

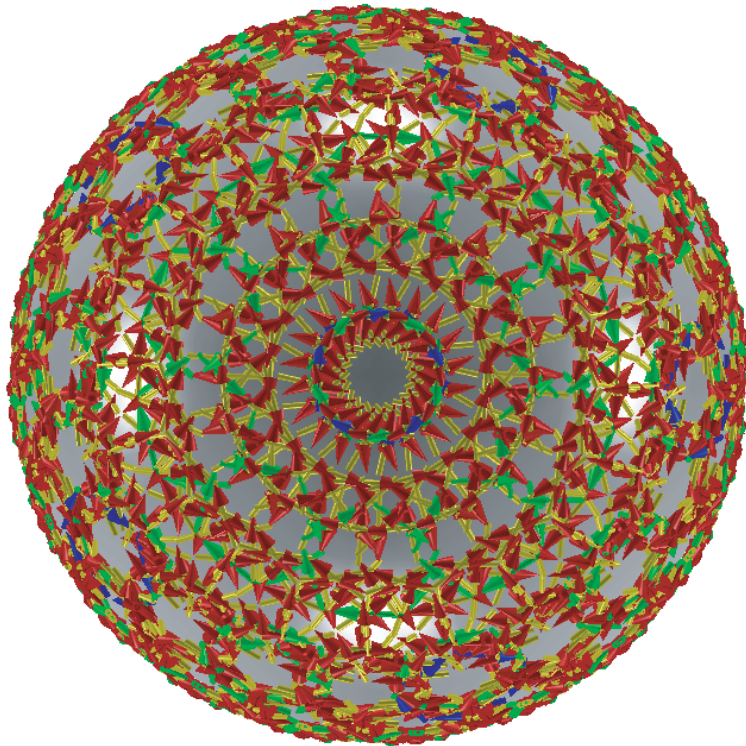


(b) Elliptic linear congruence based subdivision scheme.

Fig. 11. 1st step of the presented subdivision schemes.



(a) 600-cell based subdivision scheme.



(b) Elliptic linear congruence based subdivision scheme.

Fig. 12. 2^{nd} step of the presented subdivision schemes.

Acknowledgment

This research was carried out as part of the project S9206-N12 which was supported by the Austrian Science Fund (FWF).

References

- [1] Baumgardner, J.R., Frederickson, P.O., *Icosahedral Discretization of the Two-Sphere*. SIAM Journal on Numerical Analysis 22 (6), 1107–1115, 1985.
- [2] Buckminster Fuller, R., Geodesic Dome. United States Patent 2682235, U.S. Patent Office, June 29, 1954.
- [3] Coxeter, H.S.M., Regular Polytopes. Dover Publications, 3rd edition, 1973.
- [4] Hofer, M., Pottmann, H., Energy-Minimizing Splines in Manifolds. Transactions on Graphics 23 (3), 284–293, 2004.
- [5] Hofer, M., Pottmann, H., Ravani, B., From curve design algorithms to the design of rigid body motions. The Visual Computer 20 (5), 279–297, 2004.
- [6] Hopf, H., Über die Abbildungen der dreidimensionalen Sphäre auf die Kugelfläche. Math. Ann. 104, 637–665, 1931.
- [7] Merlet, J.-P., Parallel Robots. Springer, 2nd edition, 2006.
- [8] McCarthy, J.M., Introduction to Theoretical Kinematics. MIT Press, 1990.
- [9] Müller, H.R., Sphärische Kinematik. VEB Dt. Verlag der Wissenschaft, 1962.
- [10] Nawratil, G., Pottmann, H., Ravani, B., Generalized Penetration Depth Computation based on Kinematical Geometry. CAGD, submitted.
- [11] Pottmann, H., Wallner, J., Computational Line Geometry. Springer, 2001.
- [12] Ravani, B., and Roth, B., Mappings of spatial kinematics. ASME J. of Mech., Trans., and Auto. in Des. 106 (3), 341–347, 1984.
- [13] Schaefer, S., Hakenberg, J., Warren, J., Smooth Subdivision of Tetrahedral Meshes. Eurographics Symposium on Geometry Processing (R. Scopigno, D. Zorin, eds.), 151–158, 2004.
- [14] Stephanos, C., Sur la theorie des quaternions. Math. Ann. 22, 589–592, 1883.
- [15] Zhang, L., Kim, Y., Manocha, D., A Fast and Practical Algorithm for Generalized Penetration Depth Computation. Robotics: Science and Systems Conference (RSS07), 2007.
- [16] Zhang, L., Varadhan, G., Kim, Y., Manocha, D., Generalized Penetration Depth Computation. ACM Solid and Physical Modeling Conference (SPM06), 173–184, 2006.